

Molecular design for tuning electronic structure of π -conjugated polymers containing fused dithienobenzimidazole units



Koji Takagi ^{a,*}, Tomoharu Kuroda ^a, Masanori Sakaida ^a, Hyuma Masu ^b

^a Life Science and Applied Chemistry, Graduate School of Engineering, Nagoya Institute of Technology, Gokiso, Showa, Nagoya, 466-8555, Japan

^b Center for Analytical Instrumentation, Chiba University, 1-33 Yayoi, Inage, Chiba, 263-8522, Japan

ARTICLE INFO

Article history:

Received 29 August 2016

Received in revised form

4 November 2016

Accepted 8 November 2016

Available online 9 November 2016

Keywords:

π -Conjugated polymer

Oxidation

Protonation

ABSTRACT

Three dithienobenzimidazole derivative monomers (**M1**, **M2**, and **M3**) were prepared, where **M3** was obtained by the oxidation of **M1** and identified by the X-ray crystallographic analysis. π -Conjugated homopolymers (**P1-0**, **P2-0**, and **P3-0**) and copolymers (**P1-2**, **P3-1**, and **P3-2**) were synthesized by the palladium-catalyzed coupling polymerizations of **M1**, **M2**, and **M3**. The absorption spectra of the reference compounds (fused **R1** and non-fused **R2**), in conjunction with the optimized ground state structure, certified the importance of the fused dithienobenzimidazole skeleton to increase the effective conjugation length of the polymers. On the basis of the absorption and emission spectra of the π -conjugated polymers in CHCl_3 , the influence of the thiophene-*S,S*-dioxide as well as the comonomer structure were investigated to find out that **P3-0** and **P3-2** exhibited peak maxima at the relatively longer wavelength region due to the donor-acceptor interaction. In addition, the protonation of the imidazole imine group further tuned the optical properties of the π -conjugated polymers by promoting the charge transfer interaction along the polymer main chain, which was supported by the theoretical calculations in detail.

© 2016 Elsevier Ltd. All rights reserved.

1. Introduction

Optoelectronic devices fabricated from organic materials have many advantages over inorganic silicon-based devices owing to the light-weight and flexible characteristics, low-cost and mild manufacturing processes, and the finely tunable energy level of frontier molecular orbitals (FMOs). π -Conjugated polymers are promising candidates with the potential application to large area displays, wearable sensors, and stretchable memories. For example, bulk heterojunction solar cells comprised of π -conjugated polymer donor and fullerene derivative acceptor materials have attracted increasing attention in recent years [1–6]. However, at the present stage, organic and polymer semiconductors do not have enough performances to supersede silicon semiconductors because of the low power conversion efficiency and the short device lifetime. These parameters should be improved for the demand of commercialization. Much efforts have been devoted to the development of π -conjugated polymers with the good solution processability, the high charge carrier mobility, the broad light absorption profile, the large absorption coefficient, the appropriate

energy levels, and the favorable blend morphology. The incorporation of electron-rich and electron-deficient units, for many cases in an alternating fashion, into the polymer main chain is a reliable method to optimize the highest occupied molecular orbital (HOMO) and lowest unoccupied molecular orbital (LUMO) energy levels by virtue of the intramolecular charge transfer interaction [7–10]. These donor-acceptor architectures have been keenly studied, giving rise to many high performance devices in the recent decades.

On the other hand, the introduction of π -extended systems into the polymer backbone determines not only the electronic structure but also the intermolecular π - π stacking structure to affect the semiconducting properties of materials. The strong π - π stacking interaction leads to the good crystallinity and the high electronic conductivity in some occasions, but it reduces the polymer solubility, making the solution processability difficult in other occasions. Thus the careful choice of π -extended systems including the attachment of solubilizing groups is much important to obtain semiconducting polymers with the better performance [11]. Recently, in addition to fused ring systems consisting of the electron-rich aromatic rings (thienothiophene [12], benzodithiophene [13], naphthodithiophene [11,14], and benzotrithiophene [15,16]), those carrying both donor and acceptor constituents in one

* Corresponding author. Tel.: +81 052 735 5264.

E-mail address: takagi.koji@nitech.ac.jp (K. Takagi).

fused ring system have been investigated. For example, thiophene-fused conjugated skeletons having the electron-accepting imide group were installed in some π -conjugated polymers [17–20]. These π -conjugated polymers showed a potential utility as the field effect transistor and photovoltaic cell materials. Low band gap oligomers and polymers consisting of thiophene-fused boron dipyrromethane (BODIPY) repeat units were also synthesized [21,22]. The large overlap between HOMO and LUMO is realized to effectively lower the band gap energy, and the strong electron-accepting ability of BODIPY decreases the HOMO energy level to improve the air stability of the materials.

We have previously reported the synthesis of π -conjugated polymers based on a fused dithienobenzimidazole unit in the main chain, and found that the substitution pattern of the fused ring system as well as the chemical structure of the comonomer affect the optoelectronic characteristics of the π -conjugated polymers [23]. Imidazole has been utilized as the building unit of the π -conjugated molecules and polymers [24,25], and the transformation to imidazolium cation imparts new properties to the molecules owing to its ionic character and strong electron-accepting nature [26–29]. In this paper, we describe the chemical modification of the dithienobenzimidazole-containing π -conjugated polymers for further tuning of the electronic structure (Fig. 1). As a result, the control of FMO energy levels was possible by the choice of the comonomer, the oxidation of the thiophene ring, and the protonation of the imidazole moiety.

2. Experimental

2.1. Materials

[1,3-Bis(diphenylphosphino)propane]dichloronickel(II) [Ni(dppp)Cl₂] was purchased from Tokyo Chemical Industry. Tetrakis(triphenylphosphine)palladium(0) [Pd(PPh₃)₄], 9,9-dihexylfluorene-2,7-diboronic acid, and *i*-PrMgCl solution (2.0 M in tetrahydrofuran (THF)) were purchased from Aldrich. *n*-Butyllithium solution (*n*-BuLi, 1.6 M in hexane) was purchased from Kanto Chemical. Benzo[1,2-*b*:6,5-*b'*]dithiophene-4,5-dione [30], 1,2-di(thiophen-3-yl)ethane-1,2-dione [30], benzo[2,1-*b*:5,6-*b'*]dithiophene-4,5-dione [31], and 3,3'-dihexyl-5,5'-bis(tributylstannyl)-2,2'-bithiophene [32] were prepared as reported previously. All reactions were performed under dry nitrogen atmosphere unless otherwise noted.

2.2. Instrumentations

Microwave reactions were performed on a Biotage Initiator 8 in the normal absorption level. ¹H and ¹³C nuclear magnetic resonance (¹H-NMR and ¹³C-NMR) spectra were recorded on a Bruker Avance III HD 400 FT-NMR spectrometer in CDCl₃. Melting points (Mp) were determined on a Yanagimoto micro melting point apparatus MP-500D and were uncorrected. High resolution electrospray ionization mass spectra (HR ESI-MS) were performed on a Waters Synapt G2 HDMS in the positive mode. Elemental analyses (EA) were performed on a Elementar vario EL cube. Gel permeation chromatography (GPC) analyses were carried out on a Shodex 104 system using tandem LF-404 columns (THF as an eluent, flow rate = 1.0 mL/min, 40 °C) equipped with an ultraviolet–visible (UV–vis) detector (Shimadzu SPP-20A). Number-averaged molecular weight (*M_n*) and molecular weight distribution (*M_w*/*M_n*) were determined on the basis of a calibration curve made from standard polystyrene samples and ethylbenzene. UV–vis and fluorescence spectra were recorded on a Shimadzu UV-1650 spectrophotometer and a Shimadzu RF-5300 spectrofluorometer, respectively, using a 1 cm quartz cell. Fluorescence quantum yields (QYs) in solution

were determined relative to quinine sulfate in 0.1 M H₂SO₄ with QY of 0.55. Cyclic voltammetry (CV) measurements were performed on with a potentiostat (Hokuto HZ-5000, Hokuto Denko). The working electrode (Peek-coated platinum disk) was separated from the counter electrode (platinum wire) and the Ag/Ag + reference electrode using a glass filter (G4). Polymer films were drop-cast on to a platinum electrode from their CHCl₃ solutions. All measurements were performed at room temperature (25 ± 1 °C) and nitrogen gas was used to degas the solutions before use and flowed over the solutions during experiments.

2.3. Monomer syntheses

2.3.1. 5,8-Dibromo-2-(*p*-octyloxyphenyl)-1-pentylidithieno[3',2':3,4:2'',3'':5,6]benzimidazole (M1)

Step 1: To a EtOH solution (10 mL) of benzo[1,2-*b*:6,5-*b'*]dithiophene-4,5-dione (97 mg, 0.44 mmol) were added 4-octyloxybenzaldehyde (0.15 g, 0.62 mmol) and ammonium acetate (0.17 g, 2.2 mmol), and the reaction mixture was heated to reflux overnight. After solvents were removed, CH₂Cl₂ was added and washed with water. The organic phase was dried over MgSO₄, and the crude product was purified by SiO₂ column chromatography (gradually changing the solvent composition from CH₂Cl₂ to ethyl acetate, R_f = 0.80) to give 2-(*p*-octyloxyphenyl)dithieno[3',2':3,4:2'',3'':5,6]benzimidazole as a colorless solid (0.17 g, 90% yield). Mp 236–238 °C; ¹H NMR (CDCl₃) δ ppm 0.84–0.93 (m, 3H), 1.21–1.43 (m, 10H), 1.77–1.83 (m, 2H), 3.99 (brs, 2H), 6.94–7.01 (m, 2H), 7.50 (d, *J* = 4.89 Hz, 2H), 7.84 (brs, 2H), 8.04 (d, *J* = 7.09 Hz, 2H).

Step 2: To a THF solution (100 mL) of 2-(*p*-octyloxyphenyl)dithieno[3',2':3,4:2'',3'':5,6]benzimidazole (4.2 g, 9.5 mmol) was added NaH (55% oil suspension) (0.69 g, 29 mmol) and the reaction mixture was heated to reflux for 1 h. 1-Iodopentane (2.3 g, 11 mmol) was added, and the reaction mixture was heated to reflux overnight. After solvents were removed, CH₂Cl₂ was added and washed with water. The organic phase was dried over MgSO₄, and the crude product was purified by SiO₂ column chromatography (hexane:ethyl acetate = 1:3, R_f = 0.50) to give 2-(*p*-octyloxyphenyl)-1-pentylidithieno[3',2':3,4:2'',3'':5,6]benzimidazole (**R1**, reference compound) as a colorless solid (3.0 g, 61% yield). Mp 90–92 °C; ¹H NMR (CDCl₃) δ ppm 0.84–0.91 (m, 5H), 1.25–1.38 (m, 13H), 1.46–1.54 (m, 2H), 1.82–1.93 (m, 4H), 4.05 (t, *J* = 6.60 Hz, 2H), 4.50 (s, 2H), 7.06 (d, *J* = 8.56 Hz, 2H), 7.50 (d, *J* = 5.38 Hz, 1H), 7.55 (d, *J* = 5.38 Hz, 1H), 7.63–7.67 (m, 2H), 7.70 (d, *J* = 5.62 Hz, 1H), 8.04 (d, *J* = 5.38 Hz, 1H); ¹³C NMR (CDCl₃) δ ppm 13.9, 14.1, 22.1, 22.7, 26.1, 28.6, 29.2, 29.4, 29.7, 30.2, 31.8, 46.0, 68.2, 114.7, 119.9, 122.1, 122.9, 123.4, 124.4, 124.6, 128.9, 130.0, 130.3, 131.1, 136.4, 151.3, 160.1; Anal Calcd for C₃₀H₃₆N₂O₅: C, 71.39%; H, 7.19%; N, 5.55%; S, 12.71%; Found C, 72.52%; H, 8.12%; N, 4.81%; S, 11.28%.

Step 3: To a *N,N*-dimethylformamide (DMF) solution (20 mL) of 2-(*p*-octyloxyphenyl)-1-pentylidithieno[3',2':3,4:2'',3'':5,6]benzimidazole (0.10 g, 0.20 mmol) was added *N*-bromosuccinimide (NBS) (70 mg, 0.42 mmol), and the reaction mixture was stirred at room temperature overnight. After solvents were removed, CHCl₃ was added and washed with water. The organic phase was dried over MgSO₄, and the crude product was purified by SiO₂ column chromatography (CH₂Cl₂, R_f = 0.50) followed by recrystallization from hexane/CHCl₃ to give **M1** as a colorless solid (0.10 g, 77% yield). Mp 145–147 °C; ¹H NMR (CDCl₃) δ ppm 7.99 (s, 1H), 7.61 (d, *J* = 8.7 Hz, 2H), 7.60 (s, 1H), 7.05 (d, *J* = 8.7 Hz, 2H), 4.42 (t, *J* = 7.6 Hz, 2H), 4.05 (t, *J* = 6.5 Hz, 2H), 1.90–1.80 (4H), 1.56–1.20 (14H), 0.94–0.81 (6H); ¹³C NMR (CDCl₃) δ ppm 160.1, 151.7, 135.5, 132.4, 129.9, 129.5, 129.3, 128.4, 128.3, 126.2, 123.3, 122.7, 122.3, 116.0, 115.4, 113.1, 113.0, 68.2, 45.8, 31.9, 29.9, 29.3, 28.6, 26.1, 22.7, 22.0, 13.1; Anal Calcd for C₃₀H₃₄Br₂N₂O₅: C, 54.38%; H, 5.17%; N, 4.23%; S, 9.68%; Found: C, 54.41%; H, 5.28%; N, 4.09%; S, 9.62.

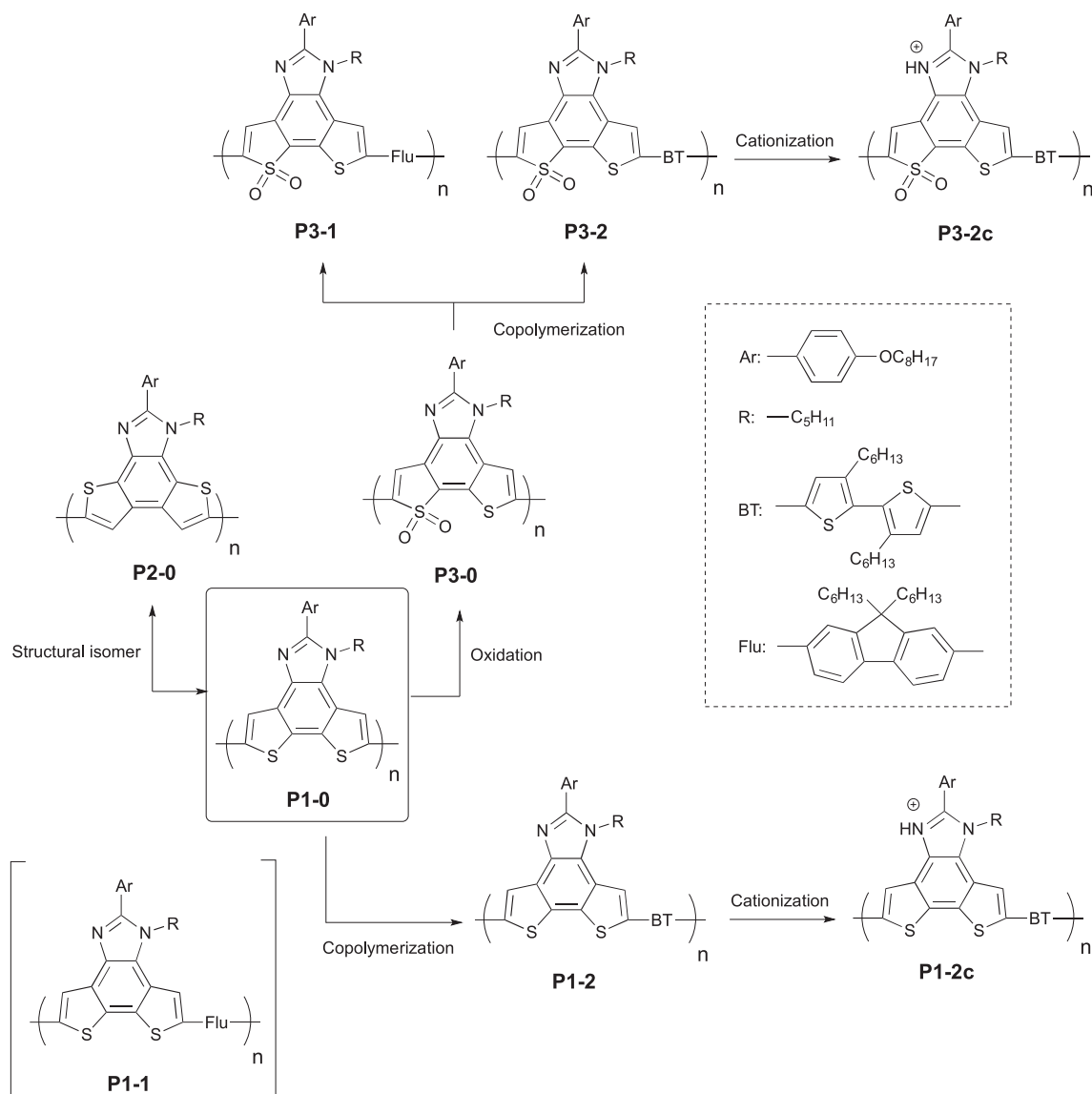


Fig. 1. Overview of dithienobenzimidazole-containing π -conjugated polymers.

2.3.2. 5,8-Dibromo-2-(*p*-octyloxyphenyl)-1-pentylthiophene-2,5-dione (M2)

This compound was synthesized from benzo[2,1-*b*:5,6-*b'*]dithiophene-4,5-dione in a similar manner to **M1**. Mp 104–106 °C; $^1\text{H NMR}$ (CDCl_3) δ ppm 7.63 (d, $J = 8.2$ Hz, 2H), 7.60 (s, 2H), 7.03 (d, $J = 8.8$ Hz, 2H), 4.33 (t, $J = 7.8$ Hz, 2H), 4.03 (t, $J = 6.6$ Hz, 2H), 1.94–1.74 (4H), 1.53–1.31 (14H), 0.95–0.82 (6H); $^{13}\text{C NMR}$ (CDCl_3) δ ppm 160.4, 152.4, 134.4, 132.3, 130.3, 130.2, 130.0, 129.9, 129.4, 129.3, 126.8, 126.5, 123.7, 123.4, 122.0, 121.8, 121.6, 116.1, 115.6, 112.5, 111.5, 68.2, 31.9, 31.3, 29.4, 29.3, 26.1, 22.7, 22.1, 13.4; Anal Calcd for $\text{C}_{30}\text{H}_{34}\text{Br}_2\text{N}_2\text{O}_3\text{S}_2$: C, 54.38%; H, 5.17%; N, 4.23%; S, 9.68%, Found: C, 54.44%; H, 5.21%; N, 4.07%; S, 9.94%.

2.3.3. 5,8-Dibromo-2-(*p*-octyloxyphenyl)-1-pentylthiophene-2,5-dione-*S,S*-dioxide (M3)

To a CH_2Cl_2 solution (40 mL) of **M1** (0.37 g, 0.55 mmol) were added 35% H_2O_2 solution (5.9 mL, 54 mmol) and 55% HCO_2H solution (23 mL, 0.11 mol) at 0 °C, and the reaction mixture was stirred at 30 °C for 18 h. After the mixture was poured into saturated NaHCO_3 solution, an aqueous phase was extracted with CH_2Cl_2 . The

organic phase was washed with water, dried over MgSO_4 , and the crude product was purified by SiO_2 column chromatography (CHCl_3 , $R_f = 0.23$) to give **M3** as a yellow solid (0.10 g, 26% yield). Mp 58–61 °C; $^1\text{H NMR}$ (CDCl_3) δ ppm 0.83–0.93 (m, 6H), 1.19–1.37 (m, 12H), 1.46–1.53 (m, 2H), 1.80–1.90 (m, 4H), 4.06 (t, $J = 6.60$ Hz, 2H), 4.45 (s, 2H), 7.08 (d, $J = 8.56$ Hz, 2H), 7.59–7.67 (m, 3H), 7.98 (s, 1H); $^{13}\text{C NMR}$ (CDCl_3) δ ppm 12.8, 13.1, 20.9, 21.6, 25.0, 27.4, 28.1, 28.2, 28.3, 28.7, 30.8, 45.2, 67.3, 75.7, 114.0, 117.5, 119.5, 120.6, 120.7, 124.3, 127.1, 128.6, 130.0, 130.1, 131.5, 155.1, 160.0; Anal Calcd for $\text{C}_{30}\text{H}_{34}\text{Br}_2\text{N}_2\text{O}_3\text{S}_2$: C, 51.88%; H, 4.93%; N, 4.03%; S, 9.23%, Found: C, 51.92%; H, 5.18%; N, 3.83%; S, 9.06%; HR ESI-MS Calcd for $\text{C}_{30}\text{H}_{35}\text{Br}_2\text{N}_2\text{O}_3\text{S}_2$ $[\text{M}+\text{H}]^+$: 695.0435, Found: 695.0431.

2.4. Synthesis of reference compound (R2)

Step 1: To a EtOH solution (2 mL) of 1,2-di(thiophen-3-yl)ethane-1,2-dione (0.20 g, 0.90 mmol) were added 4-octyloxybenzaldehyde (0.32 g, 1.4 mmol), ammonium acetate (2.1 g, 27 mmol), and *L*-proline (16 mg, 0.14 mmol). The reaction mixture was heated to reflux overnight. After solvents were

removed, CH₂Cl₂ was added and washed with water. The organic phase was dried over MgSO₄, and the crude product was purified by SiO₂ column chromatography (CHCl₃, R_f = 0.1) to give 2-(*p*-octyloxyphenyl)-4,5-di(thiophene-3'-yl)benzimidazole as a yellow solid (0.37 g, 95% yield). Mp 168–170 °C; ¹H NMR (CDCl₃) δ ppm 0.84–0.95 (m, 3H), 1.22–1.49 (m, 11H), 1.80 (s, 2H), 3.99 (t, *J* = 6.60 Hz, 2H), 6.95 (d, *J* = 8.80 Hz, 2H), 7.27–7.64 (m, 5H), 7.80 (d, *J* = 8.80 Hz, 2H), 9.08–9.34 (m, 1H); ¹³C NMR (CDCl₃) δ ppm 14.1, 22.7, 26.0, 29.2, 29.4, 31.8, 68.1, 76.7, 114.7.

Step 2: To a THF solution (5 mL) of 2-(*p*-octyloxyphenyl)-4,5-di(thiophene-3'-yl)benzimidazole (0.1 g, 9.5 mmol) was added NaH (55% oil suspension) (33 mg, 0.69 mmol), and the reaction mixture was heated to reflux for 1 h. 1-Iodopentane (54 mg, 0.27 mmol) was added, and the reaction mixture was heated to reflux overnight. After solvents were removed, CH₂Cl₂ was added and washed with water. The organic phase was dried over MgSO₄, and the crude product was purified by SiO₂ column chromatography (hexane: ethyl acetate = 1:1, R_f = 0.78) to give 2-(*p*-octyloxyphenyl)-1-pentyl-4,5-bi(thiophene-3'-yl)benzimidazole (**R2**) as an orange oil (98 mg, 85% yield). ¹H NMR (CDCl₃) δ ppm 1.05 (s, 4H), 1.25–1.48 (m, 17H), 3.82 (s, 2H), 4.01 (t, *J* = 6.60 Hz, 2H), 6.99 (d, *J* = 8.80 Hz, 2H), 7.10–7.18 (m, 3H), 7.31 (dd, *J* = 3.06, 1.34 Hz, 1H), 7.40 (dd, *J* = 2.93, 1.22 Hz, 1H), 7.50 (dd, *J* = 4.89, 2.93 Hz, 1H), 7.56 (d, *J* = 8.80 Hz, 2H); ¹³C NMR (CDCl₃) δ ppm 12.7, 13.1, 20.8, 21.6, 25.0, 27.4, 28.2, 28.4, 29.2, 30.8, 43.8, 67.1, 113.6, 118.7, 122.5, 123.6, 125.4, 125.5, 128.5, 129.4, 130.2, 135.0, 146.6, 158.6; Anal Calcd for C₃₀H₃₈N₂O₂S₂: C, 71.10%; H, 7.56%; N, 5.53%; S, 12.65%. Found C, 71.85%; H, 7.70%; N, 4.67%; S, 10.62%.

2.5. Polymerization

2.5.1. Homopolymerization (typical procedure)

A microwave vial containing **M1** (0.10 g, 0.15 mmol), bis(tri-*n*-butyltin) (92 mg, 0.16 mmol), CuI (0.86 mg, 0.16 mmol), Pd(PPh₃)₄ (8.3 mg, 7.5 μmol), THF (3.0 mL), and *N*-methylpyrrolidone (NMP) (1.5 mL) was heated under the microwave irradiation condition at 120 °C for 48 h. After CHCl₃ was added to dissolve precipitates and washing with 1 M HCl, the organic phase was dried over MgSO₄. The solution was concentrated and poured into MeOH to obtain **P1-0** as a reddish solid (67 mg, 88% yield). ¹H NMR (CDCl₃) δ ppm 0.76–1.58 (22H), 1.77–2.22 (5H), 3.88–4.57 (4H), 7.06 (3H), 7.36–8.03 (4H). Other homopolymers (**P2-0** and **P3-0**) were obtained in a similar manner.

2.5.2. Copolymerization (typical procedure)

To a THF solution (2.0 mL) of **M3** (0.10 g, 0.14 mmol) and 9,9-dihexylfluorene-2,7-diboronic acid (58 mg, 0.14 mmol) were added Pd(PPh₃)₄ (16 mg, 14 μmol) and 2 M Na₂CO₃ solution (0.5 mL, 0.96 mmol), and the reaction mixture was heated to reflux for 72 h. After CHCl₃ was added to dissolve precipitates and washing with 1 M HCl, the organic phase was dried over MgSO₄. The solution was concentrated and poured into MeOH to obtain **P3-1** as a reddish solid (41 mg, 36% yield). ¹H NMR (CDCl₃) δ ppm 0.54–1.47 (43H), 1.80–2.25 (8H), 4.09 (2H), 4.49–4.68 (2H), 7.12 (2H), 7.36–8.30 (10H). Other copolymers (**P1-2** and **P3-2**) were obtained in a similar manner.

2.6. Theoretical calculation

Theoretical calculations were performed using the Gaussian 09 W (Revision C.01) package of program. The ground state structure was optimized with density functional theory (DFT) calculation at the B3LYP/6-31G(d,p) level of theory. Time dependent (TD)-DFT calculations were then performed at the same level to estimate the vertical excitation energies and oscillator strengths (*f*).

3. Results and discussion

3.1. Synthesis

Monomers **M1** and **M2** were prepared from the corresponding benzodithiophene-4,5-dione derivatives [30,31] by the imidazole ring formation, *N*-alkylation, and bromination sequences (Fig. 2). The synthesis of **M3** was then attempted by oxidizing **M1** under various conditions. The oxidation using 3-chloroperbenzoic acid in CH₂Cl₂ at room temperature gave a complex mixture, while the reaction using H₂O₂ in CH₃CO₂H at refluxing temperature did not consume **M1**. The oxidation using NaBO₃·4H₂O in CH₃CO₂H at 50 °C also resulted in the recovery of **M1**. Finally, **M3** was successfully obtained by the reaction with H₂O₂ in HCO₂H/CH₂Cl₂ at room temperature and purified by SiO₂ column chromatography. The HR ESI-MS and elemental analysis of the crude mixture revealed that not bithiophene-*S,S,S',S'*-tetraoxide but bithiophene-*S,S*-dioxide solely existed. In this reaction condition, the imidazole ring was probably protonated by formic acid to decrease the electron density of the fused π-electron system, and one thiophene ring was oxidized to further decrease the electron density of another thiophene ring and inhibit the complete oxidation, i.e., the formation of bithiophene-*S,S,S',S'*-tetraoxide. The single crystal of **M3** was prepared by the vapor diffusion method using CHCl₃ (good solvent) and CH₃OH (poor solvent), and subjected to the X-ray crystallographic analysis (space group = *P*-1, *Z* = 2), revealing that the thiophene ring more distant from the *N*-pentyl group is oxidized (Fig. 3). The torsion angle between the imidazole ring (A) and the 4-octyloxyphenyl ring (B) is 45°, and the fused dithienobenzimidazole unit has a completely planar structure. On the other hand, in addition to fused reference compound **R1** that is the synthetic precursor of **M1**, non-fused reference compound **R2** was prepared to investigate the effect of the fused π-conjugated skeleton. **R2** was obtained from 1,2-di(thiophen-3-yl)ethane-1,2-dione [30] by the imidazole ring formation and *N*-alkylation reactions. The structure and purity of these low molecular weight compounds were absolutely confirmed by NMR spectra and elemental analyses.

Initially, the synthesis of **P1-0** was investigated using **R1** or **M1** as a monomer. When the oxidation coupling polymerization of **R1** was conducted using FeCl₃ in CHCl₃ at 0 °C for 48 h, insoluble products in organic solvents such as CHCl₃ and THF were obtained. The strong coordination interaction between the Fe³⁺ ion and the imidazole moiety might result in the formation of physical network gel. The Yamamoto and Kumada coupling polymerizations of **M1** using nickel catalysts proceeded, however, the number-averaged molecular weight of products remained around 1500. In contrast, the Stille coupling polymerization using the (Bu₃Sn)₂, CuI, and Pd(PPh₃)₄ system in THF/NMP or in chlorobenzene at 120 °C under the microwave irradiation condition for 48 h successfully gave soluble **P1-0** in 88% yield as a reddish solid. **P2-0** (a yellow solid) and **P3-0** (a reddish solid) were likewise synthesized from **M2** and **M3**, respectively. The Suzuki coupling polymerization of **M3** with 9,9-dihexylfluorene-2,7-diboronic acid in THF/2 M Na₂CO₃ solution at the refluxing temperature for 72 h gave **P3-1**, and the Stille coupling polymerization of **M3** with 3,3'-dihexyl-5,5'-bis(tributylstannyl)-2,2'-bithiophene in toluene at the refluxing temperature for 72 h gave **P3-2**. **P1-2** was synthesized from **M1** and 3,3'-dihexyl-5,5'-bis(tributylstannyl)-2,2'-bithiophene as previously reported [23]. These copolymers showed a better solubility in organic solvents than the homopolymers due to the presence of hexyl chains in the comonomer units. **P1-0** and **P3-0** were partially soluble in THF, which is the GPC eluent, owing to the rigid framework of main chain. All polymers were isolated by the reprecipitation of the CHCl₃ soluble fraction into MeOH. The number-averaged molecular weight and the molecular weight distribution of the π-conjugated

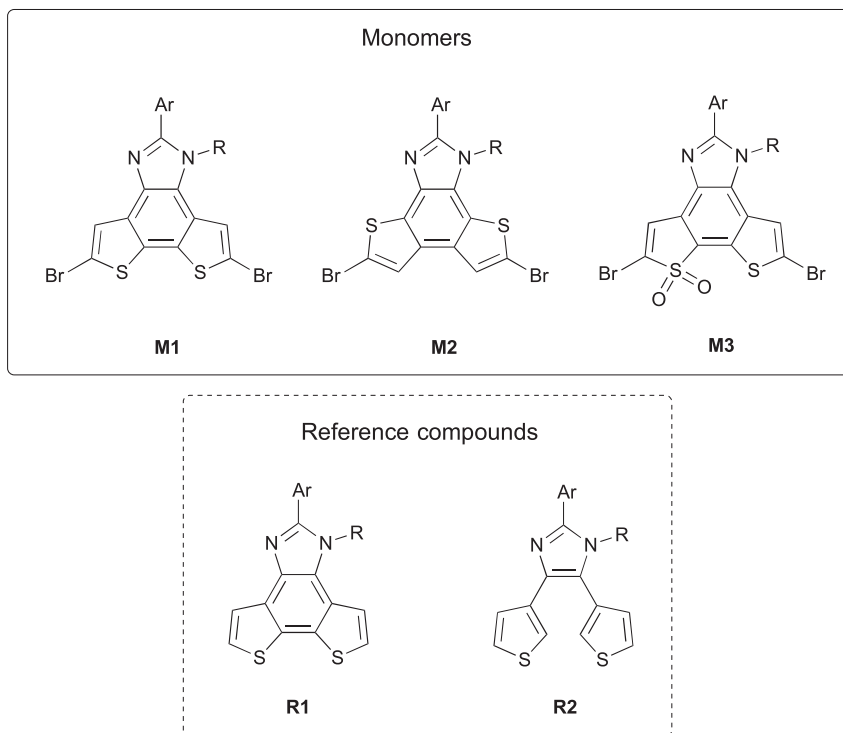


Fig. 2. Chemical structure of monomers and reference compounds (for Ar and R groups, See Fig. 1).

polymers are summarized in Table 1. Unfortunately, the molecular weights were rather low, which might be ascribed to the coordination of the imidazole to the palladium complex to decrease the catalytic activity in the polymerization.

3.2. Optical properties

At the beginning, the UV–vis absorption spectra of reference

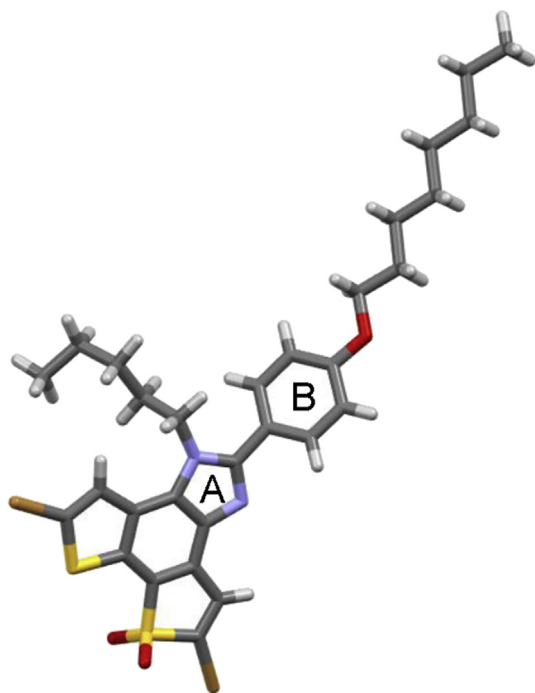


Fig. 3. Single crystal X-ray structure of **M3** in a stick model.

compounds **R1** and **R2** were measured in CHCl_3 solution (Fig. S1, a). The absorption maximum of fused **R1** exhibited a clear red-shift of 61 nm as compared with non-fused **R2**. The DFT calculations were performed for optimizing the ground state structures of 2-(*p*-methoxyphenyl)-1-methyldithieno[3',2':3,4:2'',3'':5,6]benzimidazole (**R1'**) and 2-(*p*-methoxyphenyl)-1-methyl-4,5-bi(thiophene-3'-yl)benzimidazole (**R2'**). Therein, the long alkyl substituents were replaced by the methyl group to reduce the computation time. As a result, the torsion angles between imidazole ring (A) and the thiophene ring (C) of **R1'** are 0.8° and 0.3° indicating the almost planar structure, while those of **R2'** are 14.4° and 129.4° reflecting the remarkably twisted conformation (Fig. S1, b). These results agree well with the UV–vis absorption data, and the fused dithienobenzimidazole unit incorporated in the π -conjugated polymer is expected to increase the effective conjugation length.

The UV–vis absorption and fluorescence emission spectra of three homopolymers **P1-0**, **P2-0**, and **P3-0** were then measured in CHCl_3 (Fig. 4, left). The absorption spectrum of **P3-0** was particularly broad. **P3-0** might be composed of segments with various effective conjugation lengths because the thiophene and thiophene-*S,S*-dioxide rings are supposed to be not regularly arranged

Table 1

Yield, number-averaged molecular weight, and molecular weight distribution of π -conjugated polymers.

Code	Yield (%) ^a	M_n (DP) ^b	M_w/M_n ^b
P1-0	88	4000 (7.5) ^c	1.64
P2-0	43	3300 (6.2)	1.34
P3-0	89	6700 (11.9) ^c	1.88
P1-2	49	7300 (8.4)	1.77
P3-1	36	9000 (10)	1.93
P3-2	59	8000 (8.9)	2.50

^a Isolated yield after precipitating the CHCl_3 soluble fraction into MeOH.

^b Estimated by GPC (THF as an eluent, calibrated by polystyrene standard samples). DP = Degree of polymerization calculated based on the M_n values.

^c Only soluble part in THF.

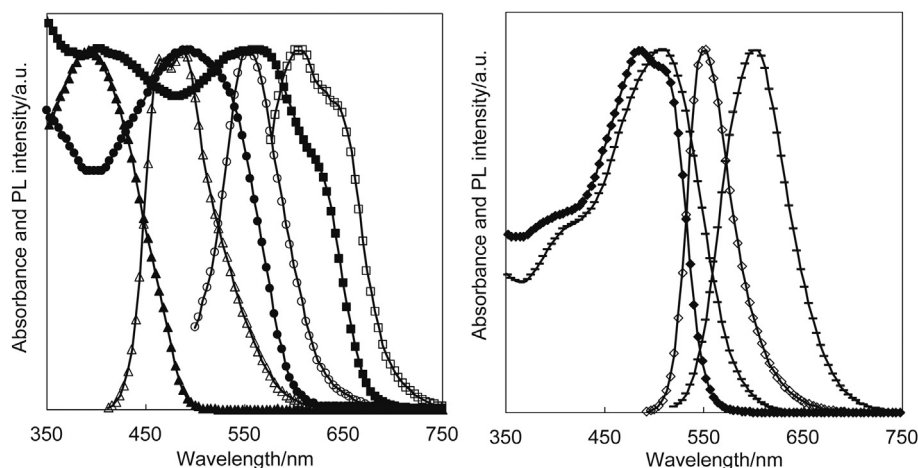


Fig. 4. UV–vis absorption (closed marker) and fluorescence emission (open marker) spectra in CHCl_3 (10^{-5} M). Left: **P1-0** (circle), **P2-0** (triangle), and **P3-0** (square). Right: **P3-1** (diamond) and **P3-2** (bar).

along the polymer main chain [33]. Two bromine atoms in monomer **M3** must have a different electronic character; namely, one is substituted on the thiophene ring and another is substituted on the thiophene-*S,S*-dioxide ring. It can be considered, however, that the Stille coupling polymerization does not proceed in the regio-controlled manner because of the small difference between two bromides in the reactivity. The absorption maximum wavelengths of **P1-0**, **P2-0**, and **P3-0** were 497 nm, 392 nm, and 569 nm, respectively. Because the thiophene rings in **P1-0** are connected with each other at the 2,5-positions, the π -conjugation is effectively expanded as compared with **P2-0**. As for **P3-0**, the charge transfer interaction between the electron-donor (thiophene) and the electron-acceptor (thiophene-*S,S*-dioxide) possibly results in the wide conjugation system. The emission maximum wavelengths exhibited a red-shift in the order of **P2-0** (488 nm), **P1-0** (554 nm), and **P3-0** (601 nm). The fluorescence quantum yield of **P2-0** was 10%, while those of **P1-0** and **P3-0** were not available because of the large overlap of the absorption spectra with the emission (small Stokes shifts), leading to the weak fluorescence intensity. Table 2 summarizes the absorption and emission maximum wavelengths along with the optical band gap energies calculated from the onset of UV–vis absorption spectra.

The UV–vis absorption and fluorescence emission spectra of **P3-1** and **P3-2** were likewise measured in CHCl_3 (Fig. 4, right). **P1-1** (See Fig. 1) composed of two thiophene rings and the fluorene unit in the main chain showed the absorption and emission maxima at 449 nm and 541 nm, respectively, as we reported in the previous paper [23]. **P3-1** is also composed of the similar main chain

structure (two thiophene rings and a fluorene unit) to **P1-1**. Because the absorption and emission maxima of **P3-1** were observed at 485 nm and 550 nm, respectively, the electronic influence of thiophene-*S,S*-dioxide included in the fused dithienobenzimidazole unit is prominent to obviously increase the effective conjugation length. **P3-2** exhibited the absorption and emission spectra at the longest wavelength region ($\lambda_{\text{ab}} = 510$ nm and $\lambda_{\text{em}} = 602$ nm) among the synthesized π -conjugated polymers, reflecting the enhanced donor-acceptor interaction. Fig. S3 visualizes the fluorescence emission color of the selected copolymers in CHCl_3 which can cover the wide optical wavelength region.

The DFT calculations were performed for the model compounds of the repeat units of **P3-1** and **P3-2**, where the long alkyl substituents were replaced by the methyl group. The optimized ground state structure indicates that **P3-1'** has larger torsion angles (28° and 25°) than **P3-2'** (17° and 15°) between thiophene or thiophene-*S,S*-dioxide rings (C) and phenyl or thienyl rings (D) (Fig. 5). On the basis of the TD-DFT calculation, important electronic transitions are always from HOMO to LUMO, and these FMO surfaces are distributed throughout the fused dithienobenzimidazole unit. The alkoxyphenyl group at the 2-position of the imidazole ring has little electronic interaction with the fused dithienobenzimidazole unit. The vertical excitation energy and oscillator strength of **P3-1'** are 2.93 eV (423 nm) and 0.62, respectively, while those of **P3-2'** were 2.72 eV (455 nm) and 0.74. The calculated excitation energies are estimated at the relatively shorter wavelength region, however, the low energy shift from **P3-1** to **P3-2** is nicely reproduced by the theoretical calculation.

The electrochemical properties of polymers were evaluated by the CV measurement. Polymer films were prepared by the drop-cast on to a platinum electrode from their CHCl_3 solutions. In all cases, the irreversible oxidation CV curves were obtained (Fig. S6). Only **P3-0** showed an irreversible reduction CV curve. The HOMO energy level (E_{HOMO}) is estimated from the onset oxidation potential (E_{onset}) using the following equation: $\text{HOMO} = -(E_{\text{onset}} + 4.73)$ eV, where the energy level is calibrated against the ferrocene/ferrocenium couple (Fc/Fc^+ measured as 0.08 V vs Ag/Ag^+) and 4.8 eV is the energy level of Fc under vacuum. Table 2 summarizes the experimental E_{HOMO} as well as the LUMO energy level (E_{LUMO}) calculated from the optical band gap (E_g) in the UV–vis absorption spectra. The E_{LUMO} for **P3-0** was alternatively estimated from the onset reduction potential, showing good agreement with that calculated from the optical band gap. Among three homopolymers, **P3-0** shows the E_{LUMO} value at the most negative level, which can

Table 2
Optical and electrochemical properties of polymers.

Code	λ_{abs} (nm) ^a	λ_{em} (nm) ^b	E_g (eV) ^c	E_{HOMO} (eV) ^d	E_{LUMO} (eV) ^e
P1-0	497	554	2.00	−5.32	−3.32
P2-0	392	488	2.48	−5.06	−2.58
P3-0	569	601	1.77	−5.51	−3.74 (−3.86) ^f
P1-2	449	541	2.23	−5.46	−3.23
P3-1	485	550	2.15	−5.73	−3.58
P3-2	510	602	1.98	−5.69	−3.71

^a Absorption maximum wavelength in CHCl_3 (10^{-5} M).

^b Emission maximum wavelength in CHCl_3 (10^{-5} M).

^c Optical band gap energy calculated from the onset of UV–vis absorption spectra.

^d Estimated from the onset oxidation potential.

^e LUMO is estimated by $E_{\text{LUMO}} - \text{HOMO} = E_g$.

^f Estimated from the onset reduction potential.

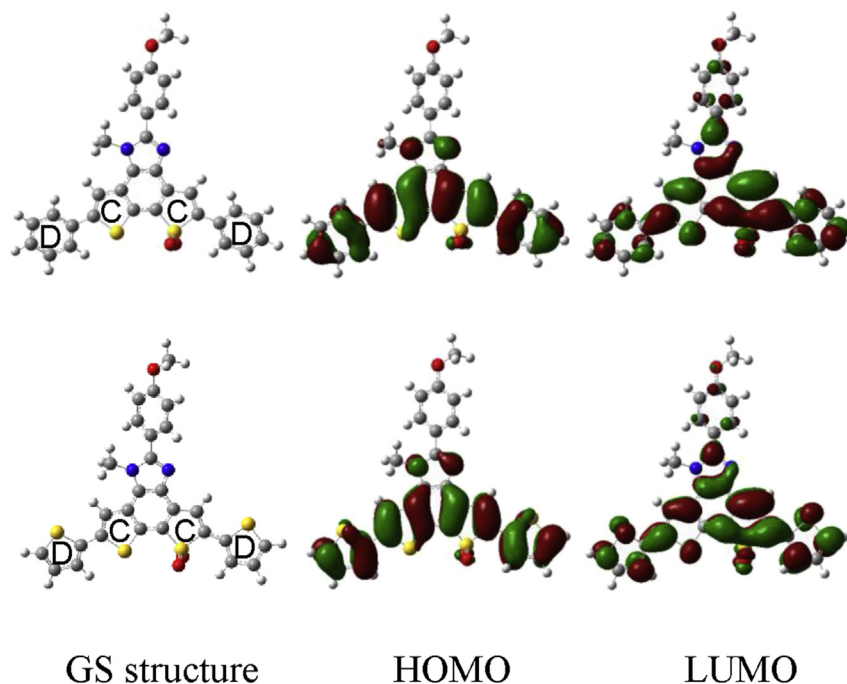


Fig. 5. Ground state (GS) structure, HOMO surface, and LUMO surface of **P3-1'** (top) and **P3-2'** (bottom).

be stemmed from the strong electron-accepting characteristic of the thiophene-*S,S*-dioxide unit. On the other hand, **P3-1** has the lower E_{HOMO} value and the higher E_{LUMO} one than **P3-2**, which are in good accordance with the trend observed in the DFT calculation; E_{HOMO} and E_{LUMO} of **P3-1** are -5.41 eV and -2.12 eV, E_{HOMO} and E_{LUMO} of **P3-2** are -5.26 eV and -2.25 eV.

Finally, the tuning of optical properties were investigated by the protonation of the fused dithienobenzimidazole unit. The imine ($\text{C}=\text{N}$) groups of **P1-2** and **P3-2** were protonated using trifluoroacetic acid (TFA) in CHCl_3 . Judging from the rough titration experiment, the spectral change was saturated by adding 50 equivalent of TFA to the dithienobenzimidazole unit in **P1-2**, while 1000 equivalent of TFA was required to completely protonate the $\text{C}=\text{N}$ group in **P3-2**. This difference might be stemmed from the decreased electron density of the imine nitrogen of **P3-2** due to the electron-withdrawing characteristic of the thiophene-*S,S*-dioxide ring. Fig. 6

shows the UV–vis absorption and fluorescence emission spectra of **P1-2** and **P3-2** before and after adding the excess amounts of TFA, which leads both polymers to exhibit several nm (in absorption) and ca. 20 nm (in emission) red-shifts of the spectra. **P1-2c** (proton-adduct of **P1-2**) has the absorption and emission maxima at 452 nm and 564 nm, respectively, while **P3-2c** (proton-adduct of **P3-2**) has them at 519 nm and 620 nm, respectively. It is noteworthy that the *N*-protonation causes the larger red-shifts than the *N*-methylation [23], which is likely originated from the smaller steric hindrance of the proton, less disturbing the π -conjugation, in comparison to the methyl group. Furthermore, the red-shifts observed for **P1-2c** and **P3-2c** are in contrast with the result reported by Carter et al. [34], where poly(2-alkyl-benzimidazole-*alt*-9,9-dihexylfluorene) exhibits a blue-shift by the proton doping using TFA. Although the torsion angle between the imidazole and the aryl group at the 2-position must increase upon protonating the $\text{C}=\text{N}$ groups in **P1-2**

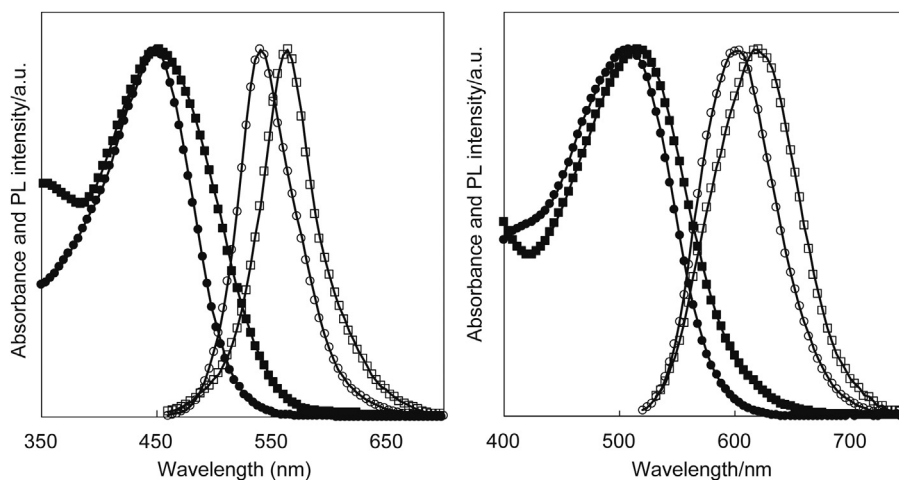


Fig. 6. UV–vis absorption (closed marker) and fluorescence emission (open marker) spectra of **P1-2** (left) and **P3-2** (right) in CHCl_3 (10^{-5} M) before (circle) and after (square) adding TFA (50 and 1000 equiv. relative to the $\text{C}=\text{N}$ group for **P1-2** and **P3-2**, respectively).

and **P3-2**, the enhanced charge transfer interaction between the electron-donor (the bithiophene comonomer unit) and the electron-acceptors (the dithienobenzimidazolium and dithienobenzimidazolium-*S,S*-dioxide cations) might result in the red-shifts of the spectra in our case. On the other hand, no obvious red-shifts were observed for **P3-1** bearing the weakly electron-donating fluorene comonomer (Fig. S2).

The DFT and TD-DFT calculations were carried out for **P1-2'** and **P3-2'**, which are the model compounds of **P1-2** and **P3-2**, respectively. Figs. S4 and S5 show the GS structures, the FMO surfaces related to the important vertical excitation, and the simulated absorption spectra before and after the proton doping event. The torsion angle between the imidazole ring (A) and the 4-methoxyphenyl ring (B) is increased from 35° to 41° irrespective of the fused dithienobenzimidazole skeleton after the proton doping, which is undoubtedly ascribed to the increment of steric repulsion. On the other hand, the averaged torsion angles between the thiophene or thiophene-*S,S*-dioxide rings (C) embedded in the fused segment and the attached thiophene rings (D) exhibits small but unambiguous decrease from 16° (**P3-2'**) to 11° (**P3-2c'**). The corresponding change of torsion angle is subtle in the case of **P1-2'** versus **P1-2c'**. The TD-DFT calculation indicates that **P1-2c'** exhibits the electronic transition from HOMO to LUMO having the peak at 476 nm ($f = 0.23$) in addition to the peak at 384 nm (from HOMO to LUMO+1, $f = 0.74$). The lower energy transition was observed as the shoulder peak. Meanwhile, the electronic transition from HOMO to LUMO of **P3-2c'** (519 nm, $f = 0.47$) was obviously shifted to the longer wavelength region as compared with that of **P3-2'** (455 nm, $f = 0.74$). The clear red-shift observed for **P3-2c'** can be ascribed to the electron-withdrawing characteristic of the thiophene-*S,S*-dioxide unit.

4. Conclusions

We herein investigated the systematic synthesis of the π -conjugated homopolymers and copolymers, containing the fused dithienobenzimidazole units, along with the low molecular weight reference compounds. The UV–vis absorption spectra in solution and the theoretical calculations of the reference compounds revealed the importance of the fused skeleton to elongate the effective conjugation length. The oxidation of the thiophene ring brought about the large red-shifts of the absorption and emission spectra, which is stemmed from the donor-acceptor interaction induced by the electron-withdrawing characteristic of the thiophene-*S,S*-dioxide unit. The protonation of the imidazole imine nitrogen was found to promote the charge transfer interaction along the polymer main chain, resulting in the red-shifts of the spectra. We believe that these findings can be an important guideline for tuning the electronic structure of π -conjugated polymers.

Note

The authors declare no competing financial interest.

Acknowledgement

Prof. Kazutake Takada and Mr. Shun-ya Yamamoto are acknowledged for the CV measurement.

Appendix A. Supplementary data

Supplementary data related to this article can be found at <http://dx.doi.org/10.1016/j.polymer.2016.11.013>.

References

- [1] H. Zhou, L. Yang, W. You, Rational design of high performance conjugated polymers for organic solar cells, *Macromolecules* 45 (2012) 607–632.
- [2] Y. Li, Molecular design of photovoltaic materials for polymer solar cells: toward suitable electronic energy levels and broad absorption, *Acc. Chem. Res.* 45 (2012) 723–733.
- [3] C.J. Brabec, S. Gowrisanker, J.J.M. Halls, D. Laird, S. Jia, S.P. Williams, Polymer-fullerene bulk-heterojunction solar cells, *Adv. Mater.* 22 (2010) 3839–3856.
- [4] A. Facchetti, π -Conjugated polymers for electronics and photovoltaic cell applications, *Chem. Mater.* 23 (2011) 733–758.
- [5] P.M. Beaujuge, J.M.J. Fréchet, Molecular design and ordering effects in π -functional materials for transistor and solar cell applications, *J. Am. Chem. Soc.* 133 (2011) 20009–20029.
- [6] C.J. Brabec, B.N. Sariciftci, J.C. Hummelen, Plastic solar cells, *Adv. Funct. Mater.* 11 (2001) 15–26.
- [7] R.C. Coffin, J. Peet, J. Rogers, G.C. Bazan, Streamlined microwave-assisted preparation of narrow-bandgap conjugated polymers for high-performance bulk heterojunction solar cells, *Nat. Chem.* 1 (2009) 657–661.
- [8] E. Wang, L. Wang, L. Lan, C. Luo, W. Zhuang, J. Peng, Y. Cao, High-performance polymer heterojunction solar cells of a polysilafluorene derivative, *Appl. Phys. Lett.* 92 (2008), 033307–1–3.
- [9] J. Hou, H.-Y. Chen, S. Zhang, R.I. Chen, Y. Yang, Y. Wu, G. Li, Synthesis of a low band gap polymer and its application in highly efficient solar cells, *J. Am. Chem. Soc.* 131 (2009) 15586–15587.
- [10] Y. Zhang, J. Zou, H.-L. Yip, Y. Sun, J.A. Davies, K.-S. Chen, O. Acton, A.K.-Y. Jen, Conjugated polymers based on C, Si and N-bridged dithiophene and thienopyrroledione units: synthesis, field-effect transistors and bulk heterojunction polymer solar cells, *J. Mater. Chem.* 21 (2011) 3895–3902.
- [11] I. Osaka, Y. Houchin, M. Yamashita, T. Kakara, N. Takemura, T. Koganezawa, K. Takimiya, Contrasting effect of alkylation on the ordering structure in isomeric naphthodithiophene-based polymers, *Macromolecules* 47 (2014) 3502–3510.
- [12] I. McCullough, M. Heeney, M.L. Chabinyc, D. DeLongchamp, R.J. Kline, M. Cölle, W. Duffy, D. Fischer, D. Gundlach, B. Hamadani, R. Hamilton, L. Richter, A. Salleo, M. Skunov, D. Sparrowe, S. Tiemey, W. Zhang, Semiconducting thienothiophene copolymers: design, synthesis, morphology, and performance in thin-film organic transistor, *Adv. Mater.* 21 (2009) 1091–1109.
- [13] H. Pan, Y. Li, Y. Wu, P. Liu, B.S. Ong, S. Zhu, G. Xu, Low-temperature, solution-processed, high-mobility polymer semiconductors for thin-film transistors, *J. Am. Chem. Soc.* 129 (2007) 4112–4113.
- [14] I. Osaka, T. Abe, S. Shimamura, K. Takimiya, Impact of isomeric structure on transistor performance in naphthodithiophene semiconducting polymers, *J. Am. Chem. Soc.* 133 (2011) 6852–6860.
- [15] X. Guo, S.R. Puniredd, M. Baumgarten, W. Pisula, K. Müllen, Benzotrithiophene-based donor-acceptor copolymers with distinct supramolecular organization, *J. Am. Chem. Soc.* 134 (2012) 8404–8407.
- [16] B.C. Schroeder, S. Rossbauer, R.J. Kline, L. Biniek, S.E. Watkins, T.D. Anthopoulos, I. McCullough, C.B. Nielsen, Benzotrithiophene copolymers: influence of molecular packing and energy levels on charge carrier mobility, *Macromolecules* 47 (2014) 2883–2890.
- [17] Y. Zhang, S.K. Hau, H.-L. Yip, Y. Sun, O. Acton, A.K.-Y. Jen, Efficient solar cells based on the copolymers of benzodithiophene and thienopyrroledione, *Chem. Mater.* 22 (2010) 2696–2698.
- [18] Y. Zou, A. Najari, P. Berrouard, S. Beaupré, B.R. Aïch, Y. Tao, M. Leclerc, A thieno [3,4-*c*]pyrrole-4,6-dione-based copolymer for efficient solar cells, *J. Am. Chem. Soc.* 132 (2010) 5330–5331.
- [19] J.A. Letizia, M.R. Salata, C.M. Tribout, A. Facchetti, M.R. Ratner, T.J. Marks, *n*-Channel polymers by design: optimizing the interplay of solubilizing substituents, crystal packing, and field-effect transistor characteristics in polymeric bithiophene-imide semiconductors, *J. Am. Chem. Soc.* 130 (2008) 9679–9694.
- [20] H. Wang, Q. Shi, Y. Lin, H. Fan, P. Cheng, X. Zhan, Y. Li, D. Zhu, Conjugated polymers based on a new building block: Dithienonaphthalimide, *Macromolecules* 44 (2011) 4213–4221.
- [21] S.G. Awuah, J. Polreis, V. Birader, Y. You, Singlet oxygen generation by novel NIR BODIPY dyes, *Org. Lett.* 13 (2011) 3884–3887.
- [22] R. Yoshi, H. Yamane, K. Tanaka, Y. Chujo, Synthetic strategy for low-band gap oligomers and homopolymers using characteristics of thiophene-fused boron dipyrromethene, *Macromolecules* 47 (2014) 3755–3760.
- [23] K. Takagi, M. Sakaida, K. Kusafuka, T. Miwa, Synthesis and optoelectronic properties of conjugated polymers based on a dithienobenzimidazole unit in the main chain, *J. Polym. Sci. Part A Polym. Chem.* 52 (2014) 401–409.
- [24] I. Nurulla, A. Tanimoto, K. Shiraishi, S. Sasaki, T. Yamamoto, Preparation of π -conjugated polymers consisting of 2-decylbenzimidazole and thiophene units and chemical properties of polymers, *Polymer* 43 (2002) 1287–1293.
- [25] T. Yamamoto, K. Sugiyama, T. Kanbara, H. Hayashi, H. Etori, Preparation and properties of *p*-conjugated poly(benzimidazole-4,7-diyl)s, *Macromol. Chem. Phys.* 199 (1998) 1807–1813.
- [26] M. Toba, T. Nakashima, T. Kawai, Synthesis, optical and electrochemical properties of arylenevinylene-based *p*-conjugated polymers with imidazolium units in the main chain, *J. Polym. Sci. Part A Polym. Chem.* 49 (2011) 1895–1906.
- [27] M. Toba, T. Nakashima, T. Kawai, Phenyleneethynylene- and

- thienyleneethynylene-based π -conjugated polymers with imidazolium units in the main chain, *Macromolecules* 42 (2009) 8068–8075.
- [28] T. Terashima, T. Nakashima, T. Kawai, Engineering control over the conformation of the alkyne-aryl bond by the introduction of cationic charge, *Org. Lett.* 9 (2007) 4195–4198.
- [29] A.J. Boydston, C.S. Pecinovsky, S.T. Chao, C.W. Bielawski, Phase-tunable fluorophores based on benzobis(imidazolium) salts, *J. Am. Chem. Soc.* 129 (2007) 14550–14551.
- [30] F.A. Arroyave, C.A. Richard, J.R. Reynolds, Efficient synthesis of benzo[1,2-*b*:6,5-*b'*]dithiophene-4,5-dione (BDTD) and its chemical transformations into precursors for *p*-conjugated materials, *Org. Lett.* 14 (2012) 6138–6141.
- [31] A. Meyer, E. Sigmund, F. Luppertz, G. Schnakenburg, I. Gadaczek, T. Bredow, S. Jester, S. Höger, Syntheses and properties of thienyl-substituted dithienophenazines, *Beilstein J. Org. Chem.* 6 (2010) 1180–1187.
- [32] A.A. El-Shehawy, N.I. Abdo, A.A. El-Barbary, J.-S. Lee, Alternating copolymers based on 2,1,3-benzothiazole and hexylthiophene: positioning effect of hexyl chains on the photophysical and electrochemical properties, *Eur. J. Org. Chem.* 25 (2011) 4841–4852.
- [33] The Chemical Structure of P3–0 Depicted in Fig. 1 is Tentatively Illustrated.
- [34] J.D. Harris, C. Mallet, C. Mueller, C. Fisher, K.R. Carter, Synthesis and characterization of poly(2-alkylbenzimidazole-*alt*-9,9-dihexylfluorene)s: a dually dopable polymer system, *Macromolecules* 47 (2014) 2915–2920.